Applied Physics A (2025) 131:171
https://doi.org/10.1007/s00339-025-08297-1

Polyethylene Terephthalate (PET) Recycling: Gamma irradiation impact on crystallinity, chemical structure and thermal stability

Izzuddin Mohd Zaharuddin[1,2] · Mohd Hafiz Mohd Zaid[1] · Mohd Hamzah Harun[2] · Yazid Yaakob[1] · Nor Batrisya Ismail[2]

Received: 30 October 2024 / Accepted: 24 January 2025 / Published online: 5 February 2025

Abstract
This study explores the effects of Cobalt-60 gamma irradiation at underexplored low-doses of 0, 20, and 80 kGy on the crystallinity, chemical structure, and thermal stability of waste polyethylene terephthalate (PET). Characterization techniques, including XRD, Raman spectroscopy, DSC, and TGA, revealed that gamma irradiation modify crystallinity and thermal stability, but overall chemical characteristic is unchanging. At 20 kGy, the crystallite size increased from 59 Å to 63 Å, the melting temperature (T_m) rose from 246.2 °C to 248.4 °C, and thermal degradation and decomposition occurred 25 °C slower. XPS data showed significant chemical restructuring, with an increase in the C/O ratio from 2.89 to 4.53, indicating the breakdown of ester linkages. These findings demonstrate that optimized gamma irradiation can potentially serve as a viable pre-treatment method to improve PET recyclability, enhance crystallinity, thermal stability, and reduce energy consumption and byproduct formation in chemical recycling processes, highlighting its potential for sustainable PET waste management.

Keywords PET · Irradiated plastic · Degradation · Recycling · Gamma irradiation

1 Introduction

A semicrystalline thermoplastic polymer called polyethylene terephthalate (PET) known for its excellent mechanical and chemical resistance. These characteristics make it typically used material in various applications, including synthetic fibers, food packaging, and water bottles [1, 2]. It is also ordinary plastic that is most frequently discovered in landfills across the world, mostly from mineral water and carbonated beverage bottles [3]. PET has become a high-priority recycling target because of the low diffusion coefficient of PET makes it suitable as a recycled material. PET is recyclable and resistance to impact, moisture, alcohols, and solvents due to the stable benzene aromatic ring in the structure [4]. In Europe, 5 million tons of plastic waste is mechanically recycled and around 50,000 tons of plastic is chemically recycled [5]. Most of PET going through mechanical recycling due to the low diffusion coefficient [6]. The collected PET waste is sorted, washed, melted into pellets or granules which then be reuse, reform or remold to other products [7]. As for chemical recycling, PET is depolymerized to reusable monomer with pyrolysis (thermolysis).

However, not like polyolefins plastic (e.g., polypropylene, and polyethylene) that producing valuable hydrocarbon products, PET mixing in the feed will harm and degrade the process and product quality due to the ester and complex aromatic compound of PET [8]. Solvent extraction method like glycolysis, hydrolysis, and methanolysis are deployed to fully depolymerize PET into its monomer constituents terephthalic acid, dimethyl terephthalate, bis(hydroxylethylene) terephthalate (BHET), and ethylene glycol [9]. Nevertheless, unwanted byproduct like ethylene acids, formaldehyde, carbon monoxide and carbon dioxide become main drawbacks to high yield of chemically recycle PET waste's product. As a result, finding innovative methods in managing recycling processes of plastic waste has become important concern. This study explores the potential employment of ionizing radiation specifically low dose gamma-ray as

✉ Mohd Hafiz Mohd Zaid
mhmzaid@upm.edu.my

[1] Department of Physics, Faculty of Science, Universiti Putra Malaysia (UPM), Serdang, Selangor 43400, Malaysia

[2] Radiation Processing Technology Division, Malaysian Nuclear Agency, Bangi, Kajang, Selangor 43000, Malaysia

pre and post-treatment in both mechanical and chemical recycling of PET.

Gamma irradiation is a form of ionizing radiation that has been extensively studied for its effects on polymers. It involves the exposure of materials to gamma rays, which can induce various chemical and physical changes within the polymer matrix [10]. The primary mechanism by which gamma irradiation affects polymers is through the generation of free radicals, which can lead to chain scission or crosslinking, depending on the irradiation dose and conditions. Irradiation technologies such as gamma rays, electron beams (e-beams), and X-rays have gained attention for their ability to modify polymer properties, including PET. These high energy ionizing techniques play a crucial role in sterilization, altering physical properties, and enhancing material performance across diverse industrial and research applications [11, 12]. When applied to PET, these methods induce significant molecular changes, including crosslinking, chain scission, and molecular cleavage, which can result in both degradation and performance enhancement [13]. Gamma irradiation, typically from cobalt-60 sources, is known for its deep penetration and uniform dose distribution, making it effective for bulk sterilization and material modification [14]. Conversely, electron beam irradiation provides higher dose rates and faster processing times, leading to unique degradation and crosslinking behaviours at varying doses. X-ray irradiation operates through different photon energy interactions, influencing the polymer's response [15].

At lower doses, gamma irradiation can enhance the crosslinking of polymer chains, resulting in improved mechanical properties and thermal stability [16]. At doses of 10–20 kGy, while gamma radiation is widely used as sterilizing method for plastic packaging, gamma radiation also has shown to reduce antimicrobial activity such as Esherichia coli, Staphylococcus aureus, and Salmonella typhimirium [17, 18]. However, at higher doses, the degradation of polymer chains becomes predominant, leading to a decrease in molecular weight and crystallinity [19]. Most of the studies have concentrated on high irradiation doses ranging from 100 kGy to 5 MGy, where chain scissions typically the dominant effect, contributing to the reductions in molecular weight and crystallinity [20–22]. Only a limited number of studies have investigated the effects of lower irradiation doses on PET, where increase in crystallinity have been reported, but not comprehensively correlating with improved mechanical strength and thermal stability [23, 24]. Furthermore, no prior research has explored the potential application of irradiation in the recycling process.

Given the importance of developing more sustainable and efficient methods for managing PET waste, this study aims to systematically investigate the impact of gamma irradiation on the crystallinity, chemical structure, thermal stability of PET and discuss the potential implementation of gamma radiation in recycling industry. A comprehensive analysis was conducted using various characterization techniques, including Field Emission Scanning Electron Microscopy (FESEM) to assess surface morphology changes post-irradiation. Fourier Transform Infrared (FTIR) Spectroscopy, X-ray Photoelectron Spectroscopy (XPS), and Raman Spectroscopy analyzed chemical composition alterations, focusing on crosslinking and degradation [25]. X-ray Diffraction (XRD) and Differential Scanning Calorimetry (DSC) examined crystallinity and thermal stability, while Thermogravimetric Analysis (TGA) evaluated thermal degradation of PET after irradiation.

Table 1 Symbols used for subsequent dosage

Symbol	Final Dosage (kGy)
PET-0	0
PET-20	23.1
PET-80	80.9

2 Experimental

2.1 Material

The polyethylene Terephthalate (PET) used in this study was sourced from PET clear bottles used for mineral drinking water. Most of the drinking bottles have density of 1.15 g/cm^3. Before utilization, the bottles were washed, dried and crushed by a crusher machine. The crushed PET size ranges between 1 and 3 mm.

2.2 Gamma irradiation of PET

The PET is prepared in 3 LDPE zip lock packets, with approximately 5 g of PET in each packet. Two samples were then irradiated with 20 and 80 kGy of Cobalt-60 Gamma Irradiation at MINTec-SINAGAMA, Malaysian Nuclear Agency, Malaysia. Doses of 20 and 80 kGy were chosen to explore the threshold between crosslinking and chain scission, based on prior studies that report significant molecular changes within this range. The radiation dose results are shown in Table 1, with the symbols used in the manuscript.

2.3 Characterization

The properties of the recycled PET and all the irradiated samples were studied via several tests. X-ray diffraction (XRD) of a PAN Analytical X'pert PRO MPD with Cu Kα1 radiation source (λ = 1.5406 Å), operating at 45 Kv and 40 mA to study the crystallinity degree of the samples. Field emission scanning electron microscopy (FESEM) (Carl

Zeiss GeminiSEM 500-70-22) was used to acquire information about the morphological changes after irradiation. The samples were required to have a metallic layer by sputter coating with platinum to undergo FESEM testing and avoid faulty images due to the collection of electrons in nonmetallic samples [26]. The analysis of potential molecular structure changes after irradiation was carried out by Fourier transform infrared (FTIR) and Raman spectroscopy. FTIR spectra of the samples were measured by the ATR technique using an FTIR spectrophotometer (Bruker Tension II). The Raman spectra of the samples before and after irradiation were recorded using a Renishaw Centrus InVia instrument equipped with a Leica microscope and an electrically refrigerated CCD camera. A wavelength of 785 nm was used as the laser wavelength, and spectra were acquired using a 50x magnification objective. X-ray photoelectron spectroscopy (XPS) was employed to analyze compositional changes on the surface of PET after irradiation. A monochromatic X-ray source from Al–Kα (hni = 1486.7 eV) with a Nexsa G2 (Thermo Fisher Scientific) was used. The survey spectra, deconvoluted C1s core line, valence band spectra, and atomic concentration with respect to the C/O ratio were acquired. Differential Scanning Calorimeter (DSC) was carried out on Netzsch DSC300 at 30 °C/min under a flowing nitrogen gas at a rate of 40mL/min to study the crystallinity degree of the samples. Thermogravimetric analysis (TGA) was used to record the percentage of weight loss during heating to a certain temperature. All figures were processed and generated by using OriginPro.

3 Results and discussions

3.1 X-ray diffraction (XRD)

The crystalline structural change and the crystal lattice parameters of the irradiated PET can be determined by XRD. Figure 1 show the XRD patterns of PET before and after being irradiated with gamma. The spectra show a peak around 2θ = 25.5° which corresponding to the (100) diffraction plane [27]. Among samples, PET-20 shows the highest peak intensity at (100) plane which is significantly higher compared to PET-0 and other samples. The higher peak intensity generally suggests a higher degree of crystallinity or the formation of new crystalline area in the sample [28]. After 20 kGy, the peak intensity decreases back around its initial value which indicates the crystalline sites are transformed back into amorphous sites. At PET-20, the spectra also show the appearance of new peak at 2θ = 22.9° corresponding to the (110) plane which then starting to disappear again in higher dose. Interestingly, PET-20 spectra peak intensity is contradictive with other study which suggest no significance different or immediate reduced peak intensity after being irradiated with gamma [21, 24]. It is found that

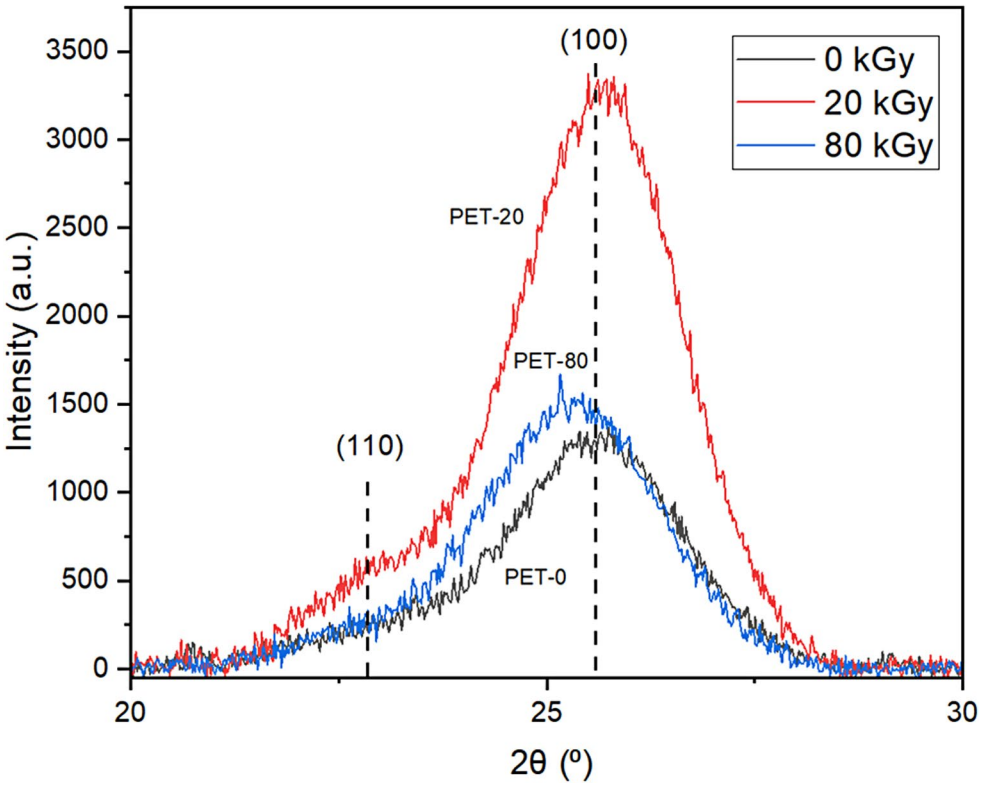

Fig. 1 X-ray diffraction pattern of PET samples before and after different gamma irradiations

Table 2 Summary of crystallite size (L) calculation based on (100) plane peak

Sample	2θ (°)	FWHM (°)	Crystallite Size, L (Å)
PET-0	25.5	2.64	59
PET-20	25.7	2.53	63
PET-80	25.3	2.65	58

this peak showing the same character as thermal treatment study of PET [29].

The full width at half maximum (FWHM) from the spectral also recorded on Table 2 which, a small narrowing of FWHM for PET-20 can be observed. The crystallite size, L for the investigated samples is also presented on Table 6 by using Scherrer's relation as below:

$$L = \frac{K\lambda}{w \times cos\theta}$$

where λ is the wavelength of the X-rays beam, w is the full width at half maximum of the peak (FWHM), 2θ the position of the main diffraction peak and K a proportionality constant with a value close to 1. Crystallite size of PET increase from 59Å to 63Å at 20 kGy and decrease back to 58Å at 80 kGy. It is also worthy to note that at 20 kGy, the position of the peak shows a light shift to higher value from its initial, which also supported the increase crystallinity of PET-20 [30].

3.2 Morphology of the surface

The microscale image of the surface before and after irradiation are shown in Fig. 2. The FESEM results show that all the PET surfaces have high surface roughness, which could be produced from the PET crushing process. Only subtle changes can be observed, for example, for PET-20, the surface become smoother and for PET-80, the surface roughness increases with the number of adhered particles on the surface. The increased roughness and crater depth observed at 80 kGy may correspond to surface cleavage and indicating localized molecular restructuring. These distinctions of the surface could come from the chain scission effect, which is a very common effect of gamma ray irradiation on the polymer [31]. The roughness can also be related to the change in crystallinity and surface modification of the PET [32]. This effect can be further confirmed through chemical composition analysis.

3.3 Fourier-Transform Infrared Spectroscopy (FTIR)

FTIR is used to investigate the structural changes of polymeric materials based on the bending and stretching vibrations of functional groups on the polymer surface. Figure 3 shows the FTIR spectra of different gamma irradiation dosages of PET. All the spectra show the same peak with different intensities, which implies that the same functional groups and molecular species exist in all the samples different concentrations. The list of functional groups identified from the spectra is shown in Table 3. The absorption bands of recycled PET were detected at 2967 cm^{-1} (C-H stretching) and 1714 cm^{-1} (C=O stretching) representing carbonyl groups; 1578 and 1505 cm^{-1} (C=C stretching), representing aromatic rings; and 1241 cm^{-1} (C=O stretching), 1017 and 969 cm^{-1} (C-O-C bending) representing ester groups [24].

Radiation can cause radical formations that can evolve in chain cleavage, charge transfer, β-scission, disproponation and other ordinary ion and radical reactions, resulting in crosslink and chain scission of polymer [33]. Esters which contain oxygen are prone to breaking their bond and release radical oxygen species. The reduction in ester group intensity (1241 and 1017 cm^{-1}) supports gamma induced scission of C-O bonds, which may facilitate crosslinking and enhance crystallinity in stable regions [28]. This scission

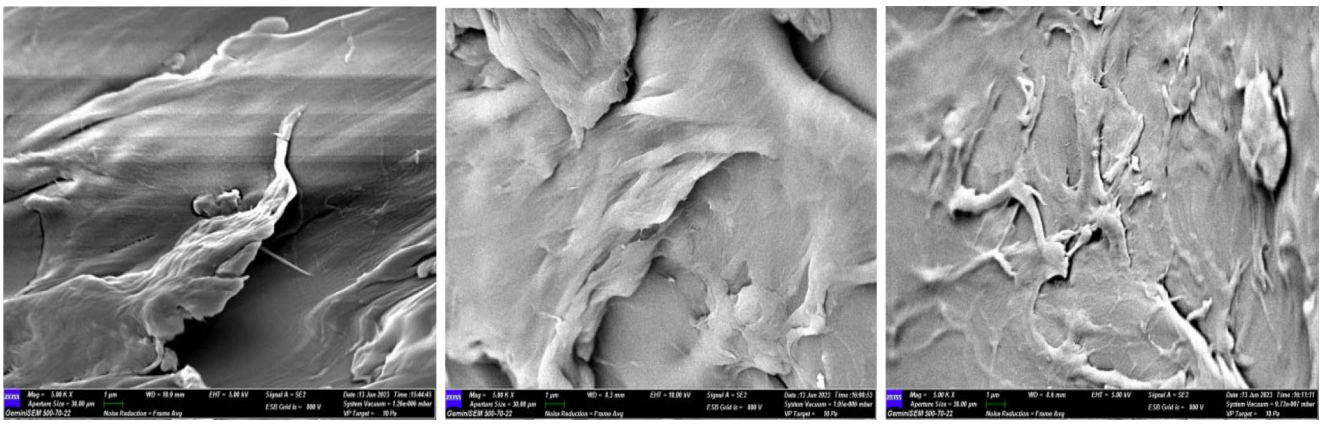

Fig. 2 SEM images of PET-0, PET-20 and PET-80 (from left to right) at 5kx magnification

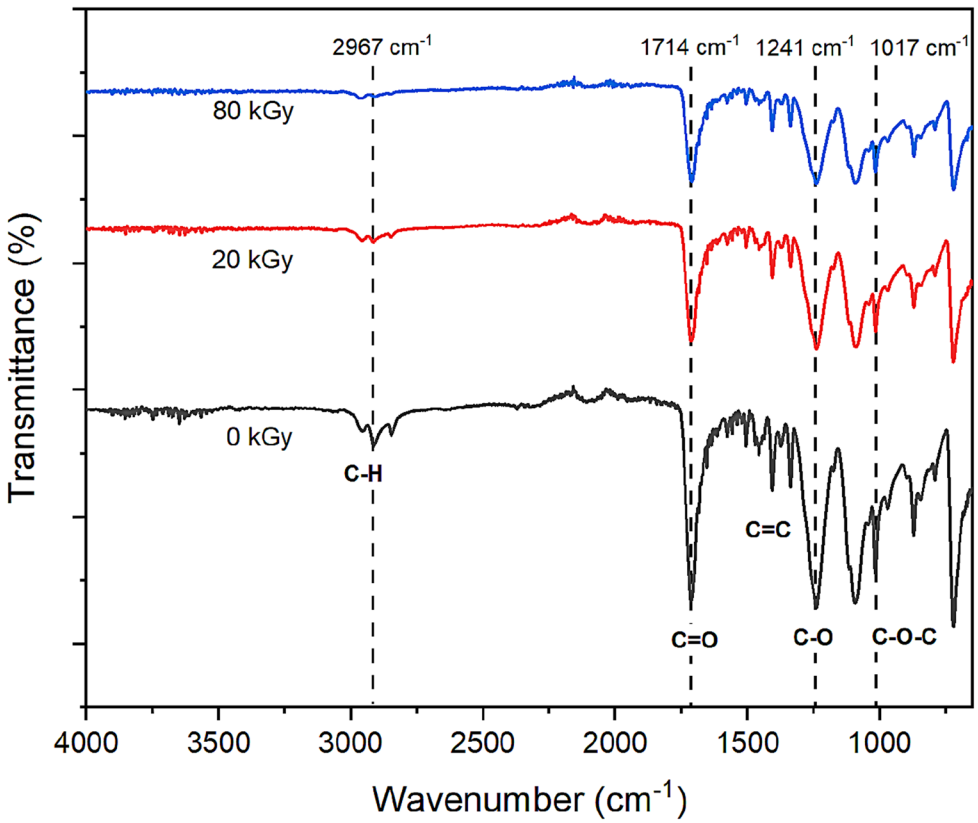

Fig. 3 IR spectra for different gamma irradiation dosage

Table 3 FTIR absorption wavenumbers of specific functional groups

Name	Location of Absorption Curve (cm^{-1})	Corresponding Species and Functional Groups	Vibration Types
C-H	2967	C-H	Stretching
C=O	1714	Carbonyl group	Stretching
C=C	1578 1505	Aromatic ring	Stretching
C-O	1241	Ester	Stretching
C-O-C	1017 969	Ester	Bending

aligns with observed changes in the C/O ratio discussed in XPS and crystallinity changes in XRD.

3.4 Raman spectroscopy

To track the chemical composition and structural changes of PET after irradiation, Raman spectroscopy was used to complement FTIR analysis. The Raman active bands of all PETs with different irradiations and their associated vibrations are summarized in Fig. 4; Table 4 [34]. All spectrums show the same characteristics and peaks but varies in the intensity of the Raman band. This difference, however, is not significant enough to alter the chemical characteristics of PET. The absence of changes in the Raman spectra except for the intensity after gamma irradiation suggests that the corresponding chemical composition did not change, at least in the Raman interaction volume, which corresponds to a sampling depth of a few micrometers.

Figure 4 reveals that the intensity of C=C band fluctuates and is not proportional to the dosage. An increase in the intensity is related to the crosslinking and branching of the matrix and the reduction in the C=C band intensity is related to damage to the PET surface [35]. Therefore, PET-20, with the higher intensity band at 1616.5 cm^{-1} compared to its unirradiated value indicates the nucleation of carbon rich cluster and decrease of the microstrain in the samples during low dose gamma irradiation. Thus, at higher dosage, PET will start to have higher microstrain and damage the polymer chains more, which will lead to surface loss and defects [36]. The findings can be demonstrated further with the correlation between Raman 1616.5 cm^{-1} band intensity and C/O ratio from XPS study. The increase in the C=C band intensity at 20 kGy indicated crosslinking and reduced strain, consistent with enhanced crystallinity and ester group reduction from XRD results.

3.5 X-ray Photoelectron Spectroscopy (XPS)

X-ray photoelectron spectroscopy revealed possible surface changes in the functional groups of the PETs. The full survey spectra of the PET samples are shown in Fig. 5(a), indicating that they were mainly composed of carbon (C)

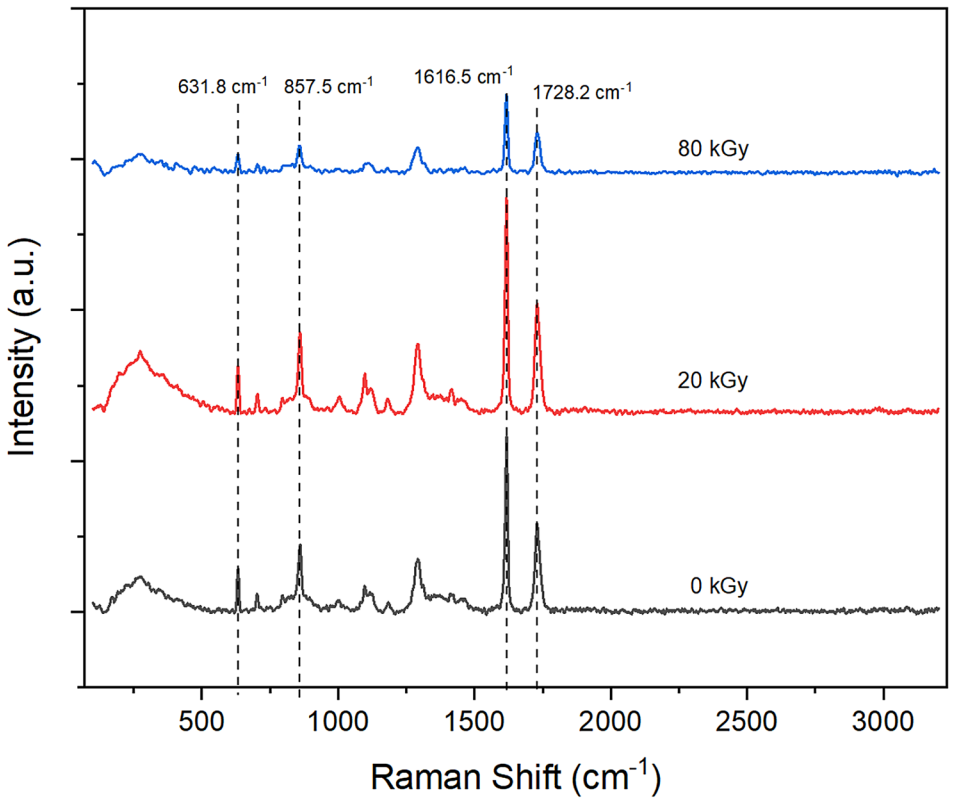

Fig. 4 Raman spectra of the PET microplastics before and after irradiation

Table 4 Raman spectral bands and corresponding molecular bands for PET

Band (cm^{-1})	Molecular Vibration
631.8	Ring Mode
857.5	Ring CC and C(O)-O stretching
1098	C-O-C anti-symmetry stretching vibration
1616.5	C=C stretching because of strong aromatic character (ring mode)
1728.2	C=O stretching, Ester compound
~3000	Vibration Benzene ring skeleton

and oxygen (O) on the PET surface. Nitrogen (N) element also detected in the minor peaks. Figure 5(b) shows the high resolution C1s XPS spectra with the identified functional groups for each peak in all the samples. Four main peaks are observed in the C1s spectrum which are present at 284.8 eV, 286.7 eV, 288.6 eV and 290.9 eV and are contributed to C-C, C-O, C=O and O=C-O, respectively, except for an extra C-N bond for PET-20 and PET-80, as presented in Fig. 5(b). The acquired main peaks are identical and complement other PET studies [37, 38]. The intensity of the peak representing C-O bonds in the C1s spectrum significantly decreased after gamma radiation of PET. This demonstrates the reduction of oxygen-containing functional groups because of the breaking of C-O bonds on the PET surface, which is also supported by the shift of the oxygen-containing functional groups peaks (C-O, C=O and O-C=O bonds) towards lower binding energies [39]. The C1s spectrum also shows the stability of carbon-carbon (C-C) bonds after irradiation, as indicated by the consistent peak intensity and firm binding energy at 284.8 eV. This stability supports the nucleation of carbon-rich clusters aligned with Raman Spectroscopy results, which may influence the mechanical and thermal properties of PET.

Table 5 shows the detectable changes in the material composition of the samples. Overall, the C/O ratios of the samples are greater after gamma irradiation and vary depending on radiation exposure. The C/O ratio significantly increased from PET-0 to PET-20, with value ranging from 2.89 to 4.53. At 80 kGy irradiation, the C/O ratio decreased to 3.23. The observed increase in the C/O ratio with the irradiation dose up to 20 kGy suggests that gamma irradiation promotes removal of oxygen containing functional groups, likely due to the breaking of C-O bonds. The amount of C-C bonds in the PET flakes also increase with irradiation dose, as shown in Table 5. An increase of the gamma irradiation dose leads to an increase generation of ketones, aldehydes, and acids moieties (O-C=O), which are directly associated with the oxidative degradation of the ester groups from the PET. The observed decrease in oxygen concentration following gamma irradiation can be attributed to its involvement in polymer oxidation and the formation of reactive oxygen

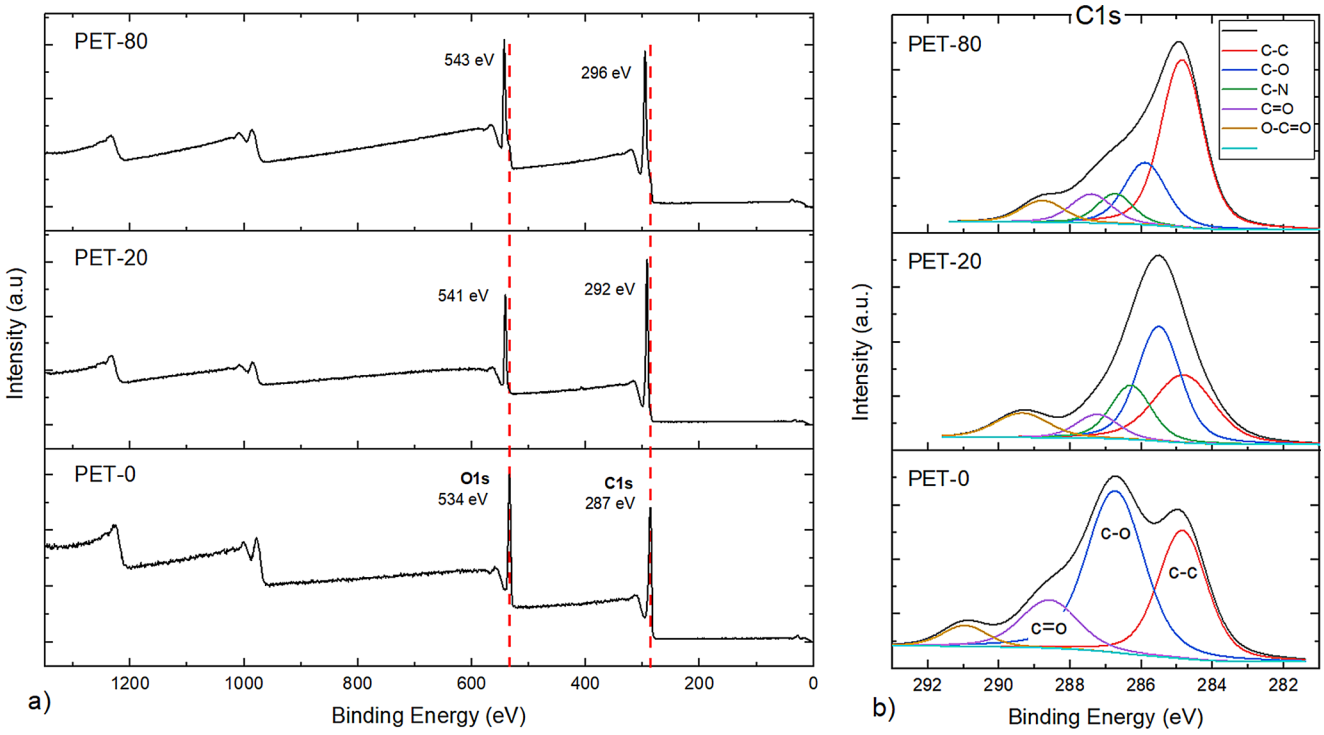

Fig. 5 (**a**) Survey spectra for all PET samples (**b**) C1s XPS spectra with fitting for PET

Table 5 Atomic concentrations of elements and moiety on the PET surface

Sample	Atomic Concentration (%)			C/O ratio	Atomic concentration per carbon bonds (%)			
	C1s	O1s	*N*		C-C	C-O	C=O	O-C=O
PET-0	74.3	25.7	-	2.89	32.6	48.19	14.32	4.86
PET-20	81.36	17.95	0.69	4.53	30.03	36.63	7.49	9.67
PET-80	76.04	23.51	0.45	3.23	51.57	21.89	16.34	10.19

species [29, 40]. The nitrogen (N) detected may originate from atmospheric adsorption due to free radical generation that can bond with reactive sites on the PET surface within the matrix [41]. The potential applications of the deoxidation process occurring in the PET are further discussed in Sect. 3.8.

3.6 Differential Scanning Calorimetry (DSC)

By using DSC thermogram, the values of enthalpy and transition temperature in the samples including information on physical damage and chemical damage were determined. Figure 6 show the DSC curve for PET-0. The DSC scan of PET showed a wide endothermic peak with a maximum at 246.2 °C, which due to the crystalline melting temperature, T_m. The melting temperature, T_m value for other samples is presented in Table 6. At PET-20 and PET-80, T_m are increased to 248.4 °C and 248.2 °C, respectively. These results showed that the thermal stability of PET after irradiation is increased in all doses, which other study agree [8].

The slight variation in T_m among the samples also suggest the changes in the crystalline structure due to irradiation.

Table 3 also showed the enthalpy of melting (ΔH_m) and crystallinity degree (X_c) changes with higher dose which was determined according to this equation:

$$X_c\,(\%) = \left(\frac{\Delta\, H_m}{\Delta\, H_{m100}}\right) \times\ 100$$

where ΔH_m is the melting enthalpy for the polymer, calculated from the area under the peak of the DSC heating curve and ΔH_{m100} is the melting enthalpy for an entirely crystalline polymer which value for 140 J/g as reported [42].

The ΔH_m is a measure of the energy required to melt the crystalline regions of the polymer. A higher ΔH_m indicates a higher degree of crystallinity. Among the samples, unirradiated PET with highest enthalpy of melting, has the highest degree of crystallinity at 32.36%. The crystallinity degree then decreased to 23.91% at PET-20 and increase to 26.15% at PET-80. The increase T_m at 20 kGy, despite lower ΔH_m, suggests improved thermal stability due to restructured

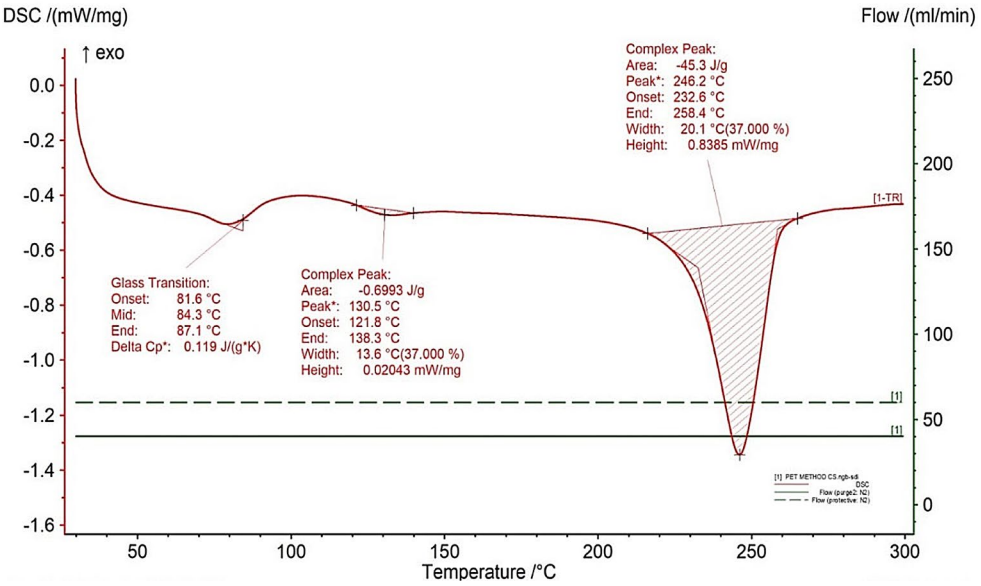

Fig. 6 DSC heating curve for PET-0

Table 6 DSC melting temperature (T_m) and crystallinity degree (X_c) calculated

Sample	T_m (°C)	ΔH_m (J/g)	X_c (%)
PET-0	246.2	45.3	32.36
PET-20	248.4	33.47	23.91
PET-80	248.2	36.61	26.15

crystalline domains, which align with enhanced crystallite size in XRD and supported by reduced amorphous signal in Raman spectroscopy [43, 44]. This suggests a reorganization of crystalline regions leading in enhanced thermal stability but lower overall crystallinity, likely due to partial amorphization of less stable regions during the heating process. Doumeng et al. (2021) also discussed the inaccuracy of using DSC for crystallinity degree measurements, emphasizing its lower accuracy compared to XRD and Raman Spectroscopy. This discrepancy arises from the polymer's complex thermal behavior, particularly the overlapping of crystallization and melting processes [45].

3.7 Thermogravimetric Analysis (TGA)

Thermogravimetric analysis (TGA) was used to assess the samples thermal stability. Figure 7 shows the TGA thermogram of the recycled PET. TGA thermograms revealed that the decomposition of the PET was a two-stage degradation. The first stage occurred in the temperature range of 200 °C attributed to quaternized graft chain degradation. The total weight loss at this stage was found to be approximately 6% of the total weight. The onset temperature of this stage in PET-0 was 30.5 °C. The major decomposition of the polymer occurred in the second stage, where the onset temperature for this stage was 375 °C for PET-0. From 375 °C to 460 °C, the weight loss dramatically decreased to 78%, which was attributed to the decomposition of the backbone polymer of PET. Figure 7 present that the TGA curves of irradiated PET shifted toward higher temperature, which have slower decomposition rate and higher decomposition temperature. For PET-20 and PET-80, the first stage of degradation occurred at 38 °C, and the major decomposition occurred from 400 °C to 500 °C. Gamma irradiation can influence the thermal degradation temperature of PET, which in this study improve the thermal stability of PET after irradiation.

3.8 Potential applications in recycling process

At studied low doses of gamma irradiation, the result from FTIR clearly show minimal impact on the chemical structure of PET, indicating that gamma irradiation does not negatively affects PET polymer matrix. This highlights the viability of gamma irradiation as pre-treatment for PET during mechanical recycling. By sterilizing the waste and simultaneously improving the crystallinity and thermal stability of PET, as demonstrated in the XRD, TGA and Raman spectroscopy results, gamma irradiation enhances the efficiency and quality of recycled materials. In the pyrolysis recycling, the presence of oxygen-containing functional groups like esters, are major contributors to the degradation of chemical recycling products quality by generating oxygenated compounds such as carbon monoxide, carbon dioxide, benzoic acid, benzaldehyde and phenol [46]. Gamma irradiation-induced deoxidation indicated by XPS results addresses this issue by reducing these oxygenated compounds thereby improving the overall chemical recycling quality, making it particularly valuable for managing blended solid plastic waste in pyrolysis or gasification recycling process [47]. This process also facilitates depolymerization and enhances

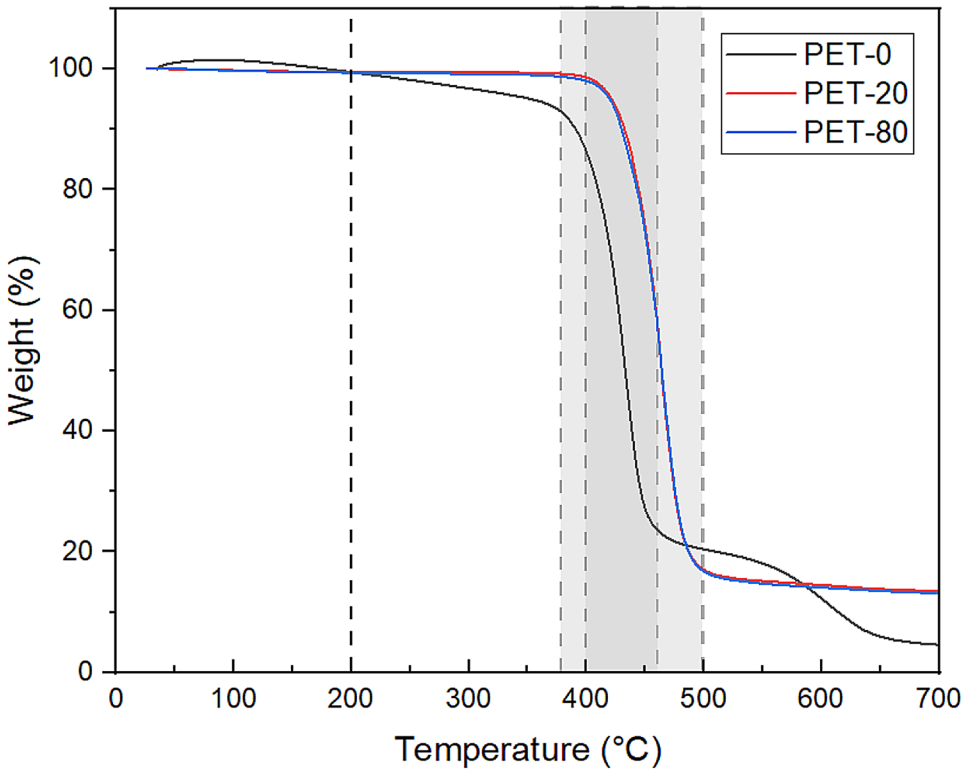

Fig. 7 TGA thermograms of the irradiated PET

the susceptibility of PET to advance recycling methods, including hydrolysis, glycolysis and methanolysis, while improving chemical recycling efficiency by reducing energy consumption and processing time [48]. Consequently, integrating gamma irradiation as a pre-treatment with thermal recycling processes, such as pyrolysis and gasification, offers a promising pathway to address both waste management and energy demands.

4 Conclusion

In this study, gamma-irradiated polyethylene terephthalate (PET) at doses of 0, 20, and 80 kGy was successfully developed, and its crystallinity, chemical structure, and thermal stability were analyzed using XRD, FTIR, Raman spectroscopy, XPS, DSC, and TGA. The results show that gamma irradiation induces significant changes in PET's crystallinity, thermal stability, and chemical composition. At 20 kGy, crystallinity and crystallite size increased, higher melting temperatures, and improved thermal stability, suggesting that crosslinking is the dominant mechanism. This is further supported by the observed reduction in oxygen-containing functional groups and increased unsaturation, indicating chemical restructuring. At higher doses, 80 kGy, chain scission becomes more prominent, leading to a reduction in crystallinity and increased degradation of polymer chains. Overall, the study underscores the potential of using gamma irradiation as a pre- or post-treatment in recycling processes, especially at low doses, where it can improve the thermal and structural properties of PET without compromising its polymer matrix. Future studies should focus on refining the irradiation parameters to further optimize the process for industrial applications, with attention to scaling up and ensuring environmental and economic feasibility.

Acknowledgements This work was supported by Strategic Research Fund (SRF), Ministry of Science, Technology, and Innovation (MOSTI), Malaysia.

Author contributions Izzuddin Mohd Zaharuddin: Formal Analysis, Investigation, Methodology, Software, Visualization, Writing– Original Draft. Mohd Hafiz Mohd Zaid: Conceptualization, Data curation, Funding acquisition, Project administration, Software, Supervision, Writing– Original Draft. Mohd Hamzah Harun: Conceptualization, Data curation, Formal Analysis, Supervision, Writing– Original Draft. Yazid Yaakob: Data curation, Formal analysis, Writing– review and editing. Nor Batrisya Ismail: Data curation, Formal analysis, Writing– review and editing.

Data availability The data are available upon request.

Declarations

Competing interests The authors declare that they have no known competing financial interests or personal relationships that could have appeared to influence the work reported in this paper.

References

1. A.K. Singh, R. Bedi, B.S. Kaith, Mater. Today Proc. **26**, 1293 (2020)
2. A. Torlakoğlu, G. Güçlü, Waste Manage. **29**, 350 (2009)
3. N.H. Mohd Nasir, F. Usman, E.L. Woen, M.N.M. Ansari, A.B.M. Supian, Saloma, Recycling 8, (2023)
4. M.N. Miranda, M.J. Sampaio, P.B. Tavares, A.M.T. Silva, M.F.R. Pereira, Sci. Total Environ. **796**, 148914 (2021)
5. M.S. Qureshi, A. Oasmaa, H. Pihkola, I. Deviatkin, A. Tenhunen, J. Mannila, H. Minkkinen, M. Pohjakallio, J. Laine-Ylijoki, J. Anal. Appl. Pyrol. **152**, (2020)
6. M. Vasylius, A. Tadžijevas, D. Šapalas, V. Kartašovas, J. Janutėnienė, P. Mažeika, Polym. (Basel). **15**, 4166 (2023)
7. V. Jamdar, M. Kathalewar, R.N. Jagtap, K.A. Dubey, A. Sabnis, Polym. Eng. Sci. **55**, 2653 (2015)
8. T.M.A. Razek, H.M. Said, M.R. Khafaga, A.W.M. El-Naggar, J. Appl. Polym. Sci. **117**, 3482 (2010)
9. Woldemar d'Ambrières, Field Actions Sci. Rep. **12** (2019)
10. A.T. Fintzou, M.G. Kontominas, A.V. Badeka, M.R. Stahl, K.A. Riganakos, Radiat. Phys. Chem. **76**, 1147 (2007)
11. S. Fares, Nat. Sci. (Irvine). **04**, 499 (2012)
12. L.S. Fifield, M. Pharr, D. Staack, S.D. Pillai, L. Nichols, J. McCoy, T. Faucette, T.T. Bisel, M. Huang, M.K. Hasan, L. Perkins, S.K. Cooley, M.K. Murphy, Radiat. Phys. Chem. **186**, (2021)
13. M.F. Zaki, J. Phys. D Appl. Phys. **41**, (2008)
14. A.W. Grzelak, S. Jeffkins, L. Luo, J. Stilwell, J. Hathcock, Biotechnol. Prog **39**, (2023)
15. N. Girard-Perier, S.R.A. Marque, N. Dupuy, M. Claeys-Bruno, F. Gaston, S. Dorey, L.S. Fifield, Y. Ni, D. Li, W.K. Fuchs, M.K. Murphy, S.D. Pillai, M. Pharr, L. Nichols, Front. Chem. **10**, (2022)
16. Y. Yin, M. Liu, X. Zheng, S.Z. Shen, P. Deng, J. Appl. Polym. Sci. **127**, 200 (2013)
17. C. Vasile, D. Pamfil, T. Zaharescu, R.P. Dumitriu, G.M. Pricope, M. Râpă, G. Vasilievici, Polym. (Basel) **14**, (2022)
18. K.M. Karina, C.M. Napolitano, S.I. Borrely, Radiat. Phys. Chem. **142**, 23 (2018)
19. A. Bahramian, Surf. Interface Anal. **53**, 215 (2021)
20. G. Burillo, L. Tenorio, E. Bucio, E. Adem, G.P. Lopez, Radiat. Phys. Chem. **76**, 1728 (2007)
21. K. Chikaoui, Radiat. Phys. Chem. **162**, 18 (2019)
22. D.H. Jeon, K.H. Lee, H.J. Park, Radiat. Phys. Chem. **71**, 1059 (2004)
23. L.H. Hao, D.T.T. Hieu, L.Q. Luan, H.T. Phuong, V. Dinh, L.A. Tuyen, P.T.T. Hong, T. Van Man, T.D. Tap, J. Appl. Polym. Sci. **139**, (2022)
24. S.G. Prasad, A. De, U. De, Int J Spectrosc 2011, 1 (2011)
25. M. Djebara, J.P. Stoquert, M. Abdesselam, D. Muller, A.C. Chami, Nucl. Instrum. Methods Phys. Res. B **274**, 70 (2012)
26. S. Lee, H. Miyaji, P.H. Geil, J. Macromolecular Sci. Part. B **22**, 489 (1983)
27. A.A. El-Saftawy, A. Elfalaky, M.S. Ragheb, S.G. Zakhary, Radiat. Phys. Chem. **102**, 96 (2014)
28. S. Siddhartha, K. Aarya, S.K. Dev, J.B.M. Raghuvanshi, Krishna, M.A. Wahab, Radiat. Phys. Chem. **81**, 458 (2012)
29. A. Szczurek, T.N.L. Tran, J. Kubacki, A. Gąsiorek, K. Startek, A. Mazur-Nowacka, R. Dell'Anna, C. Armellini, S. Varas, A. Carlotto, A. Chiasera, A. Łukowiak, J. Krzak, M. Ferrari, Mater. Chem. Phys. **306**, (2023)
30. K. Chikaoui, M. Izerrouken, M. Djebara, M. Abdesselam, Radiat. Phys. Chem. **130**, 431 (2017)
31. A. Usman, M.H. Sutanto, M. Napiah, S.E. Zoorob, S. Abdulrahman, S.M. Saeed, Ain Shams Eng. J. **12**, 271 (2021)
32. V. Kumar, Y. Ali, R.G. Sonkawade, A.S. Dhaliwal, Nucl. Instrum. Methods Phys. Res. B **287**, 10 (2012)
33. K. Awasthi, V. Kulshrestha, D.K. Avasthi, Y.K. Vijay, Radiat. Meas. **45**, 850 (2010)
34. F.J. Boer10, S.K. Bahl, G.E. Mcgraw, *Vibrational Analysis of Pol yet Hylene Tereph t Halate and Its Deuterated Derivatives* (1976)
35. N. Jin, Y. Song, R. Ma, J. Li, G. Li, D. Zhang, Anal. Chim. Acta. **1197**, 339519 (2022)
36. B. Mallick, T. Patel, R.C. Behera, S.N. Sarangi, S.N. Sahu, R.K. Choudhury, Nucl. Instrum. Methods Phys. Res. B **248**, 305 (2006)
37. O. Plohl, A. Erjavec, L. Fras Zemljič, A. Vesel, M. Čolnik, M. Škerget, Y. Van Fan, L. Čuček, G. Trimmel, J. Volmajer, Valh, J. Clean. Prod. **421**, (2023)
38. S. Ben Amor, M. Jacquet, P. Fioux, M. Nardin, Appl. Surf. Sci. **255**, 5052 (2009)
39. S. Dorey, F. Gaston, S.R.A. Marque, B. Bortolotti, N. Dupuy, Appl. Surf. Sci. **427**, 966 (2018)
40. S. KLAIMY, J.F. LAMONIER, M. CASETTA, S. HEYMANS, and S. DUQUESNE, Polym. Degrad. Stab. **187**, (2021)
41. K. Zhu, H. Jia, W. Jiang, Y. Sun, C. Zhang, Z. Liu, T. Wang, X. Guo, L. Zhu, Environ. Sci. Technol. **56**, 779 (2022)
42. A.K. Kalkar, V.D. Deshpande, B.S. Vatsaraj, Polym. (Guildf). **55**, 6948 (2014)
43. I. Kevin Eiogu, U. Ibeneme, O.M. Aiyejagbara, Am. J. Nano Res. Appl. **8**, 58 (2020)
44. S. Zhu, M. Shi, M. Tian, L. Qu, G. Chen, J. Text. Inst. **109**, 294 (2018)
45. M. Doumeng, L. Makhlouf, F. Berthet, O. Marsan, K. Delbé, J. Denape, F. Chabert, Polym. Test. **93**, (2021)
46. N. Dimitrov, L. Kratofil Krehula, A. Ptiček, Siročić, and Z. Hrnjak-Murgić, Polym Degrad Stab 98, 972 (2013)
47. M.S. Qureshi, A. Oasmaa, H. Pihkola, I. Deviatkin, A. Tenhunen, J. Mannila, H. Minkkinen, M. Pohjakallio, J. Laine-Ylijoki, J. Anal. Appl. Pyrol. **152**, 104804 (2020)
48. K. Ragaert, L. Delva, K. Van Geem, Waste Manage. **69**, 24 (2017)